Multimedia Tools and Applications
https://doi.org/10.1007/s11042-024-19460-w

Attention deficit hyperactivity disorder subtypes classification: a machine learning approach with phenotypic information and brain tissue volume

K Usha Rupni[1] · **P Aruna Priya**[1]

Received: 8 December 2023 / Revised: 7 March 2024 / Accepted: 18 May 2024

Abstract
Attention deficit hyperactivity disorder (ADHD) is a critical neurodevelopmental disorder that needs to be diagnosed and treated early to lower the risk of related health issues. This research study uses a machine-learning (ML) classification model to provide a computer-aided diagnosis method for ADHD subtypes namely ADHD-inattentive and ADHD-combined. The brain tissue volume and phenotypic information of the children are used to train the ML classification model. The grey matter and white matter brain tissues are segmented from T1-weighted brain MRI of children using a modified fuzzy c-means clustering algorithm. A novel thresholding and pixel-based volume calculation method generates volume for segmented tissues. The highest accuracy of 92.98% is achieved for classifying ADHD subtypes and typically developing (TD) with Extreme Gradient Boosting (XGBoost) classifier among the other ML classifiers. An interpretative approach provides the insight of the classification model and it predicts that medication status, intelligence quotient, gender, and grey matter volume that are used in this research are the key factors in distinguishing between ADHD subtypes and TD individuals. In conclusion, T1-weighted MRI brain tissue volume of children can help healthcare providers diagnose ADHD and its subtypes along with the symptom-based diagnosis.

Keywords Attention deficit hyperactivity disorder · Brain tissue volume · Segmentation · Machine learning · Magnetic resonance imaging · Shapley additive explanations

1 Introduction

Children are greatly affected by the brain disorder known as Attention Deficit Hyperactivity Disorder (ADHD) and it has significantly increased in recent years. The prevalence of ADHD in children of ages 3 to 12 is 7.6% and in teen of ages 12 to 18 is 5.6%

✉ P Aruna Priya
arunaprp@srmist.edu.in

[1] Department of Electronics and Communication Engineering, College of Engineering and Technology, SRM Institute of Science and Technology, Chengalpattu District, Kattankulathur, Tamil Nadu 603203, India

[1]. This disorder is a consistent pattern of impulsiveness, hyperactivity, and distraction that hinders normal functioning and development in the individual. It is categorized into three subtypes based on the Diagnostic and Statistical Manual of Mental Disorders [2]. Firstly, the predominantly inattentive (ADHD-I) subtype is primarily characterized by symptoms of inattention. Such individuals may appear to be daydreaming or forgetful and often have difficulty completing tasks or activities. Secondly, the predominantly hyperactive-impulsive (ADHD-H) subtype is primarily characterized by symptoms of hyperactivity and impulsivity. This type of child may engage in impulsive behaviors without considering the consequences. Finally, the combined (ADHD-C) subtype is characterized by inattention and hyperactivity/impulsivity symptoms. Individuals with ADHD-C exhibit a combination of the symptoms seen in the predominantly inattentive and predominantly hyperactive-impulsive. Using the ICD-10-CM, the 10th revision of the international classification of diseases, the ADHD subtype has two more categories known as unspecified type and other types along with the three subtypes [3].

ADHD individuals can exhibit varying degrees of symptom severity and impairment. The symptoms appear in a variety of contexts, including at school, work, and home which interferes with functioning to meet the diagnostic criteria for ADHD [4, 5]. Diagnosis and treatment of ADHD involve a complete assessment by a healthcare professional, who considers symptoms, history, and other appropriate factors. Individuals with ADHD can control their symptoms and improve their quality of life through a variety of intrusions, such as medication, behavioral therapy, and educational support [6, 7]. Symptoms have been the basis for the diagnosis of ADHD presently, which can change over time. Therefore, researchers are motivated to use brain imaging techniques to investigate such neurodevelopmental disorders. Recently, the investigation of brain-related disorders has made excessive use of non-invasive imaging modalities [8–11]. The most widely used technique for neuroimaging analyses is magnetic resonance imaging (MRI) as it provides scans with more details compared to other imaging techniques [12]. The important tissues in brain MRI are grey matter (GM) and white matter (WM) which play important roles in brain function [13]. Both tissues can contribute to the understanding of ADHD. However, GM is often the focus of research for ADHD.

GM consists of neuronal cell bodies and is involved in information processing, cognition, and decision-making [14]. The primary signs of ADHD, like decreased attention, impulse control, and executive functioning, are associated with the functioning of specific brain regions predominantly composed of GM. Therefore, studying GM can provide insights into the specific brain regions involved in ADHD-related difficulties. GM undergoes significant developmental changes throughout childhood and adolescence. During brain development, there is a process called synaptic pruning, where unnecessary or weak connections are eliminated, leading to a decrease in GM volume [15]. Research suggests that individuals with ADHD may experience atypical development of GM, potentially contributing to the symptoms observed in the disorder. By studying GM development, researchers can gain insights into the neural underpinnings of ADHD during critical periods of brain maturation. GM regions are rich in neurotransmitter receptors that are crucial for proper neural communication. Neurotransmitters like dopamine, norepinephrine, and serotonin are implicated in neurological disorders [16], and alterations in their receptors within GM regions may contribute to ADHD symptoms. Studying GM allows researchers to investigate the relationship between neurotransmitter systems and ADHD. GM alterations, such as differences in volume or density, may be associated with cognitive and behavioral impairments in ADHD. Identifying structural abnormalities in specific GM regions can provide insights into the neurobiological

basis of the disorder and potentially contribute to our understanding of its underlying mechanisms [17, 18].

WM abnormalities, such as alterations in microstructure or integrity, have been observed in individuals with ADHD [19]. These abnormalities may affect the efficient communication between different brain regions, potentially contributing to ADHD symptoms. However, the analysis of WM abnormalities is more complex and needs imaging modalities like diffusion tensor imaging (DTI) [20]. This inspired the investigation of typically developing (TD) and ADHD subtypes using the volume of both GM and WM tissues.

The main contributions of the study are:

i. To introduce a computer-assistant diagnosis method based on a machine learning (ML) classification model for ADHD subtypes using children's MRI and phenotypic information to help healthcare providers.
ii. Automatic segmentation of the important brain tissues is implemented based on fuzzy c-means (FCM) clustering and thresholding.
iii. The volume of the important brain tissues is calculated without the usage of online available tools.
iv. A novel sampling method is implemented to balance the classes of the dataset known as conditional oversampling.
v. Finally, an interpretative solution utilizing Shapley additive explanations (SHAP) is performed on the efficient ML-based multiclass classification model to find the most important features responsible for TD and ADHD subtypes (ADHD-I and ADHD-C) classification.

This article contains the following sections: Section 2 outlines the existing research works in ML-based ADHD classification. Section 3 discusses the suggested segmentation of brain tissues from brain MRI and the subsequent volume calculation. The ML approaches used to predict or classify ADHD subtypes are detailed in the same section. The study's findings and discussions are outlined in Sections 4 and 5, respectively. The research study concludes with the future direction and findings.

2 Related work

Several studies have utilized ML models to classify individuals with ADHD and TD using various data modalities and features. Some of the important existing works in the years 2019 to 2023 are discussed in the following:

The authors introduced a random forest (RF) method in [21] that achieved an accuracy of $0.82(\pm 0.09)$. Here, genetic and positron emission tomography (PET) imaging are utilized to differentiate between individuals with ADHD and healthy controls. This study is constrained by the lack of external validation and a small sample size of 38 participants. The authors examined three classifiers: Adaptive Boosting (AdaBoost), RF, and Support Vector Machine (SVM) [22]. Here, Electroencephalogram (EEG) signals are recorded for children while they do a cognitive task. The highest accuracy of 84% was achieved with AdaBoost. The research study [23] utilizes continuous performance test (CPT) data to classify ADHD, employing RF and neural networks as ML models. The RF method attained an accuracy of 87%. The study is limited to using only standard CPT variable samples from clinically referred children with diagnosed ADHD and little patient information. The deep

forest approach introduced [24] is a tree-based ensemble method. One-dimensional functional connectivity and three-dimensional amplitude of low-frequency fluctuations features extracted from functional MRI (fMRI) data are utilized here. The Kennedy Krieger Institute (KKI) imaging site of the ADHD-200 dataset had the best accuracy of 82.73%. The authors in [25] suggested a categorized system for ADHD by the SVM method. The fMRI functional connectivity characteristic is used for classification, achieving an average maximum accuracy of 86.43% for the Peking-2 imaging site in the ADHD-200 dataset. Three objective formulations in this scheme are based on the L1-norm. A dual subspace classification technique utilizing functional connection is introduced in [26]. Binary hypothesis testing is conducted on the ADHD_200 dataset here. This study is limited by the robustness of the parameter setting and the small sample size of children with ADHD. The author suggested classifying ADHD using the Naïve Bayes machine learning algorithm with structural MRI (sMRI) data [27]. The proposed approach attained an accuracy of 84%. The researchers in [28] utilized volumetric characteristics and cortical thickness obtained from sMRI in their research. ADHD had greater GM volume than TD individuals in fifteen brain areas. The decrease in cortical thickness occurred in 27 brain areas. Five classifiers were utilized, with radial-based SVM and linear SVM achieving the highest accuracy of 75%.

ADHD and TD classification is commonly carried out through the use of EEG, PET, and MRI with ML techniques. EEG provides the highest accuracy than other imaging modalities. But, EEG may induce seizures in children and PET is an invasive technique. Thus, MRI is the ideal imaging technique for children due to its safety and non-invasiveness. This study uses sMRI instead of fMRI because of the limited availability of fMRI in developing countries. Another significant limitation of the aforementioned study is the classification between ADHD and TD is addressed, but not for ADHD subtypes. Additionally, research on ADHD subtypes is few and mainly involves the use of EEG and fMRI [29–31]. Therefore, the proposed research will use sMRI to classify ADHD subtypes.

3 Materials and methods

This research is mainly to classify ADHD subtypes and TD efficiently using phenotypic information and volume of brain tissues obtained from T1-weighted MRI or sMRI of children. In this section, we have discussed the dataset, brain tissue segmentation, brain tissue volume calculation, important ML algorithms, and the SHAP explanation method. Figure 1 shows the flow of the study.

3.1 Data description

Brain scans of children with ADHD and TD are gathered from the ADHD-200 dataset. There are 947 T1-weighted MRI and resting-state fMRI in the dataset, among which 585 are TD and 362 are ADHD subjects. In the collection of eight imaging sites, we worked on T1-weighted MRI of children obtained from Peking University (PKU), KKI, New York University Child Study Center (NYU), and Oregon Health Sciences University (OHSU) imaging sites only as they contained both TD and ADHD subtypes along with complete phenotypic information. In the chosen imaging sites, there are 578 subjects of which TD are 318, 165 are ADHD-C, 90 are ADHD-I, and 5 are ADHD-H. The subjects utilized for the study are detailed in Table 1.

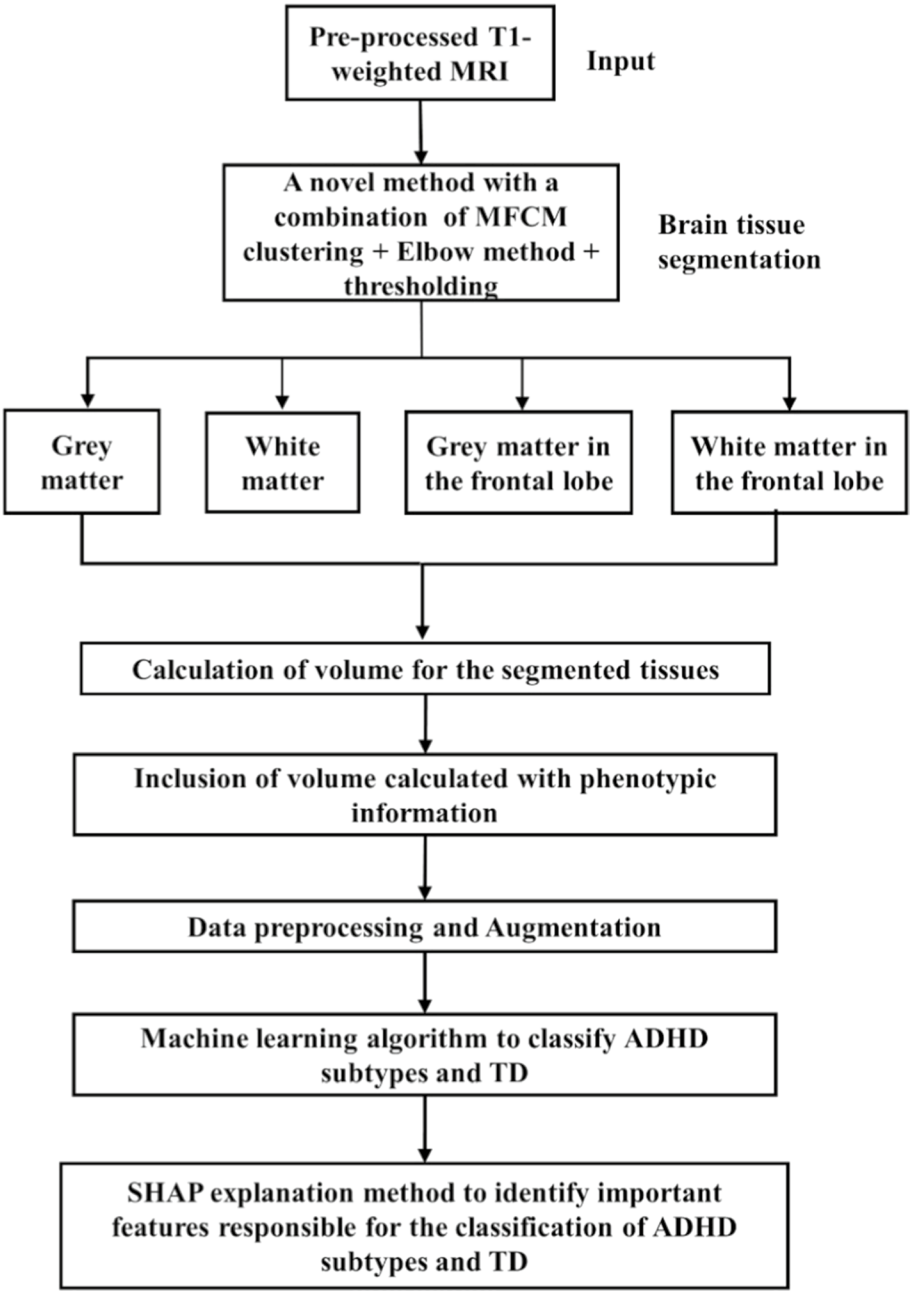

Fig. 1 Pictorial representation of the proposed study flow

The dataset repository also made preprocessed images available online by three different teams such as Athena, Neuroimaging Analysis Kit (NIAK), and Burner [32]. In this study, the Athena pipeline based on AFNI and FSL software packages is used. This preprocessing pipeline

Table 1 Description of subjects by site obtained from the ADHD-200 dataset

Imaging Site	Gender	Age range	Medication status			TD	ADHD	Total
			Medication Naive	Not Medication Naïve	Not available			
KKI	Female	8–13	29	8	0	27	10	37
	Male	8–13	39	7	0	34	12	46
NYU	Female	7–18	61	3	12	51	25	76
	Male	7–18	70	25	50	48	97	145
OHSU	Female	7–12	29	2	5	25	11	36
	Male	7–12	30	6	7	17	26	43
PKU	Female	8–16	49	1	0	45	5	50
	Male	8–17	119	25	0	71	73	144

starts with the removal of non-brain tissues [33]. Then, a non-linear wrap is done between the skull-stripped image and the Montreal Neurological Institute (MNI) space [34] using linear transform and a non-linear registration procedure [35, 36]. The skull removed brain images and smoothed by a 6 mm full width at half maximum (FWHM) Gaussian shared outputs in the repository as compressed NifTI files are used as inputs to the brain tissue segmentation.

3.2 Proposed brain tissue segmentation and volume calculation

In this study, the GM and WM tissues from the T1-weighted MRI of the brain are segmented using a novel method which is the combination of the Modified fuzzy c-means (MFCM) clustering technique, elbow method, and thresholding. The shape of the T1-weighted MRI is (197, 233, 189) which is in NifTI format and is converted to 189 slices of the two-dimensional image with shape (197, 233) for giving as input to the clustering process. The MFCM technique [37] is a variation of the standard FCM clustering algorithm. FCM is an unsupervised clustering algorithm that assigns membership degrees to each data point, indicating the degree of belongingness to each cluster. Here, additional modifications are introduced to enhance the clustering process. The optimum number of clusters is set based on the elbow method (see Fig. 2) instead of using the random values which is one of the drawbacks of existing FCM-based segmentation. The elbow method [38] is used to find the optimal number of clusters by analyzing the within-cluster sum of squares (WCSS) value, which is calculated using (1).

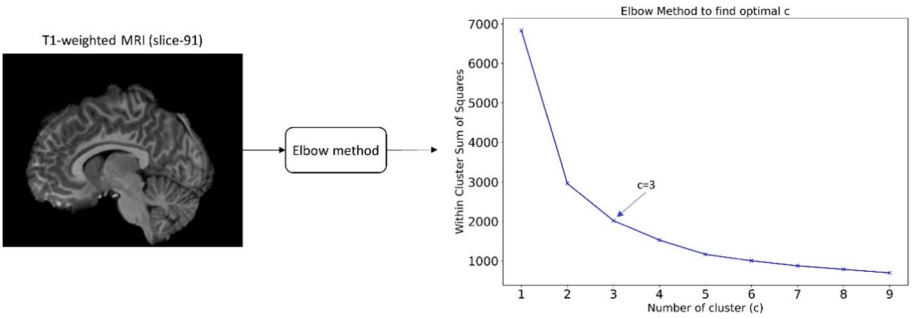

Fig. 2 Process to choose the optimal number of cluster value

$$WCSS = \sum_{P_i \text{ in } \text{Cluster } j} distance\left(P_i C_j\right)^2 \tag{1}$$

Where $distance(P_iC_j)^2$ is the sum of the squared distances between each data point and its centroid within cluster j. This distance can be calculated using a method known as Euclidean distance.

For segmenting brain tissues, the MFCM method uses spatial and grey-level interactions with the center pixel. To distinguish unreliable and reliable neighbors, the center pixels neighboring pixels perform an adaptive local window filtering which results in a filtered image that is then constructed using newly generated intensity values derived from those reliable neighbors. Then, the intensity histogram of the filtered image will be used to instantly cluster. Finally, thresholding is applied to extract the GM and WM from the clustered output brain image. The total pixels for the extracted GM and WM are calculated and the equivalent values in cubic centimeters are estimated. Similarly, the volume of GM and WM is calculated in the frontal lobe of the subjects by cropping the segmented images. In addition to other phenotypic data that are already provided with the dataset, such as age, gender, full intelligence quotient (full IQ), and medication status for each subject, the following features are added: GM volume on the whole (GMV), GM volume in the frontal lobe (GMV_F), WM volume on the whole (WMV), and WM volume in the frontal lobe (WMV_F). The data frame with all these features is further trained with the ML algorithm. The steps involved in obtaining the brain tissue volume are provided in Algorithm 1. The mathematical equations involved in the segmentation and volume calculation of brain tissues are given in the following:

1. Deviation σ_k from the median value within N_k is given by (2),

$$\sigma_k = \sqrt{\sum_{p \in N_k} \left(x_p - \bar{x}_k\right)^2 / n_k} \tag{2}$$

Where x_p is pixel p intensity level in N_k,$\bar{x}_k$ is the intensity value of the median, n_k is the count of pixels in N_k. When $x_p - \bar{x}_k$ is larger compared to σ_k then pixel p is unreliable and if lesser p is reliable.

2. Window weight coefficients, C_{kp} is given by (3),

$$C_{kp} = \begin{cases} C_{kp\_s}.C_{kp\_g}, & if\ p \epsilon N_p \\ 0, & otherwise \end{cases} \tag{3}$$

Where N_p represents the reliable neighboring set.

3. The spatial term (C_{kp_s}) and grey level term (C_{kp_g}) are defined by (4) and (5),

$$C_{kp\_s} = \begin{cases} \exp\left(-d_{kp\_s}\right), & if\ p \epsilon N_p \\ 0, & otherwise \end{cases} \tag{4}$$

$$C_{kp\_g} = \begin{cases} \exp\left(\frac{-\left\|x_k - x_p\right\|^2}{\lambda_g . \sigma_{kp\_g}^2}\right), & if\ p \epsilon N_p \\ 0, & otherwise \end{cases} \tag{5}$$

Where d_{kp_s} is the spatial Euclidean distance calculated for pixels k and p, x_k is the center pixel intensity, λ_g is the grey level effect factor, and σ_{kp_g} is the intensity deviation from the center pixel in $N_p.C_{kp\_g}$.

4. The ξ_k gives the filtered intensity of the center pixel and it is calculated using (6),

$$\xi_k = \left\{ \frac{\sum_{p \epsilon N_k} C_{kp}.x_p}{\sum_{p \epsilon N_k} C_{kp}} \right. \tag{6}$$

5. Enhanced FCM (EnFCM) algorithm [39]:
The objective function (J_s) is given by (7),

$$J_s = \sum_{i=1}^{c} \sum_{k=1}^{q} \gamma_k u_{ik}^{w} \left(\xi_k - v_i\right)^2 \tag{7}$$

Where w is a weighting exponent, $v_i$is the i^{th} cluster original value, u_{ik} is the fuzzy membership of the k^{th} pixel in cluster I, and γ_k is the number of voxels from the whole stack of slices.

6. The parameters u_{ik} and v_i values are found such that the J_s is the lowest. Thus, the Lagrange multiplier can be used to rewrite (7) and it is given by (8),

$$L_s = \sum_{i=1}^{c} \sum_{k=1}^{q} \left[\gamma_k u_{ik}^{w} \left(\xi_k - v_i\right)^2 \right] + \sum_{k=1}^{q} \lambda_k \left(1 - \sum_{i=1}^{c} u_{ik} \right) \tag{8}$$

Taking the derivative of L_s regarding u_{ik} and then v_i, and also equating to 0, we get (9) and (10):

$$\lambda_k = w \gamma_k \left[\sum_{j=1}^{c} \left(\xi_k - v_j\right)^{\frac{-2}{w-1}} \right]^{1-w} \text{ and therefore}$$

$$u_{ik} = \left[\sum_{j=1}^{c} \left(\frac{\xi_k - v_j}{\xi_k - v_j} \right)^{\frac{-2}{w-1}} \right]^{-1} \tag{9}$$

$$v_i = \left(\sum_{k=1}^{q} \gamma_k u_{ik}^{w} \xi_k \right) \left(\sum_{k=1}^{q} \gamma_k u_{ik}^{w} \right)^{-1} \tag{10}$$

7. Using the threshold method, specific brain tissues can be extracted from T1-weighted MRI scans. Here, we may accurately extract the GM and WM tissues by selecting a threshold value (T) between 30 and 100. When T is taken below 30, we are unable to retrieve GM or WM pixels accurately; whereas, when T is taken above 100, no brain tissue pixels are retrieved.

(i) To extract GM, we choose high intensity (i.e., x = 255) when x > T and x < 200, and otherwise x = 0

(ii) To extract WM, we choose high intensity (i.e., $x = 255$) when $x > T$ and $x > 150$, and otherwise $x = 0$

8. Brain tissue volume is calculated from the obtained total pixels or voxels of extracted GM or WM. The volume of brain tissues is given by (11),

$$\text{Volume}, V = T \times S \tag{11}$$

Where T is the total pixel of GM or WM and S is the slice thickness ($S = 1.3$ mm). The pixel-to-centimeter (cm) conversion is done with the condition, cm = T*(2.54/Dots Per Inch).

Algorithm 1 Algorithm of proposed brain tissue segmentation and volume calculation.

Read the preprocessed T1-weighted brain MRI

Initialize:
Number of clusters = 3 (based on the elbow method),
Fuzziness degree (m) = 2,
Number of iterations=100,
The threshold value for convergence (ε)=0.05,
Window size = 5×5,
Neighbor effect = 2.15, and
Threshold (T)= 50

Ensure: *Deviation from median value to find reliable and unreliable pixels is calculated using (2)*

The window weighting coefficient is computed from (3), (4), and (5)

Apply the adaptive local window filter and obtain the filtered image

Count the filtered image's intensity histogram using (6)

Cluster the filtered image based EnFCM algorithm's intensity histogram using (8), (9), and (10)

Apply the threshold method for the clustered output image to get the grey matter and white matter tissues

Calculate the total number of pixels for the tissues

For grey matter pixel calculation
start
if *x>T and x<200,* **then**
x=255
else
x=0
end
For white matter pixel calculation
start
if *x>T and x>150,* **then**
x=255
else
x=0
end

Obtain the brain tissue volume in cubic centimeters using (11)

3.3 Machine learning algorithms

ML algorithms are computational techniques that find the desired outputs from the inputs by learning relevant data. Recently, ensemble ML has been the preferred technique as the

main goal is to combine a set of state-of-the-art ML models to achieve better performance and reliability [40].

Some important ML algorithms utilized in the research are discussed: Gaussian Naïve Bayes (GNB) is a probabilistic classifier that applies Bayes' theorem under the assumption of feature independence. It is suitable for multiclass classification but it is constrained by issues like the zero frequency problem and potential errors in estimation under specific conditions. Bagging is an ensemble learning technique designed to enhance the stability and precision of machine learning systems. The process involves generating various subsets of the initial dataset using sampling with replacement, training individual base models on each subset, and combining their predictions to get a final prediction. The decision tree is typically the primary model employed here. Random Forest (RF) is an ensemble learning technique that leverages the power of many decision trees to attain high accuracy and flexibility in a variety of ML tasks. It is commonly utilized and appropriate for both classification and regression tasks. Extra Trees is a variation of RF that adds extra unpredictability throughout the tree construction process. It is particularly useful when computational resources are limited, or when reduced variance and faster training times are desired. Gradient Boosting (GB), AdaBoost, and eXtreme Gradient Boosting (XGBoost) are ensemble learning methods that progressively merge weak learners to form a strong learner. Adaboost functions by iteratively training a sequence of weak learners on adaptively adjusted versions of the dataset. The algorithm gives more weight to misclassified instances, enabling succeeding weak learners to focus more on challenging cases. Each weak learner is trained on a subset of the data, and their predictions are combined using a weighted sum to obtain the final prediction. GB builds an ensemble of decision trees sequentially, with each tree learning to correct the mistakes of its predecessors. It optimizes a loss function instead of instance weights like Adaboost. XGBoost is an optimized implementation of GB with several enhancements aimed at improving speed and performance. It employs a more regularized model formalization to control overfitting and has advanced features such as tree pruning, handling missing values, and parallel computing. Voting ensembles combine predictions from multiple independent models by taking a majority vote for the classification task. The three models used are SVM, logistic regression, and decision tree. Each ML algorithm possesses unique strengths and is applicable in various situations. Therefore, it is crucial to test them out and select the one that aligns best with the particular problem and dataset.

3.4 Classification of ADHD subtypes using ML algorithms

In multiclass classification, the data preprocessing and balancing of the dataset are very significant for the ML model to work efficiently. The basic data preprocessing of ML such as the removal of null values and outliers is done and then the sampling method is used to balance the dataset. The dataset now includes 489 subjects, of which 306 are for TD, 94 are for ADHD-C, and 89 are for ADHD-I, following data preparation and the removal of the extremely rare ADHD-H subtype subjects. Then, the novel sampling method called conditional oversampling is applied. The oversampling is a data augmentation method used for dealing with imbalanced datasets. Firstly, the count of the samples for each class is calculated. Then, the highest count of the class is fixed as the threshold. Finally, the minority class is doubled or tripled to match the highest count of the sample. Following the data preprocessing and balancing of the dataset, the total number of data has been augmented to 855, which is then given to the ML algorithms. The parameters and hyperparameters of the proposed study are given in Table 2. Some of the important hyperparameters of the XGBoost classifier are varied. The learning_rate is

varied between 0.01 to 0.2, colsample_bytree and subsample is varied from 0.5 to 1, and max_depth varied from 3 to 10. To determine the optimal values for hyperparameters, a grid search tuning method is performed over the specified ranges.

The efficient ML model is interpreted using Shapley additive explanations (SHAP) [41]. Shapley values are computed from coalitional game theory using the SHAP approach. It specifies the explanation given by (12),

$$g(z') = \phi_0 + \sum_{j=1}^{M} \phi_j z'_j \tag{12}$$

Where g represents the explanation model, $z' \epsilon \{0,1\}^M$ represents the coalition vector or simplified features, M represents the maximum coalition size, and $\phi_j \epsilon R$ is the feature attribution for a feature j, the Shapley values.

To compute Shaley values, simulate some feature values present and some feature values absent. If all feature values are present, then (12) can be simplified and given by (13),

$$g(z') = \phi_0 + \sum_{j=1}^{M} \phi_j \tag{13}$$

By calculating the contribution of each feature to the prediction, SHAP seeks to explain the prediction or classification of an instance or a class.

The experimental environment is a PC with 11th Gen Intel(R) Core(TM) i5-1135G7 @ 2.40GHz, 2.42 GHz, 16.0 GB RAM, an operating system of 64-bit, and a processor of ×64. The classification models were implemented using Python 3.10 software. The Python libraries used in the study are Scikit Learn, Seaborn, Matplotlib, NumPy, and Pandas. Further, the SHAP version 0.42.1 was used for classification interpretation.

4 Results

The volume calculation of GM and WM is made using 189 segmented slices from the preprocessed T1-weighted MRI. Figure 3 depicts each step in the proposed segmentation for slice number 91. The input image (see Fig. 3(a)) is initially filtered using an adaptive local window filter which eliminates noise, outliers, and unnecessary blur to get the filtered image (see Fig. 3(b)). Then, the filtered image is divided into three clusters (see Fig. 3(c)): blue for GM, yellow for WM, and dark blue for the third cluster, which is for the cerebrospinal fluid and background. The needed tissue is then extracted from the clustered image using thresholding. The thresholded GM and WM from the clustered image are shown in Figs. 3(d) and 3(e).

4.1 Analysis of the TD and ADHD subtypes in children

The data analysis of the children in the age group of 7 to18 with ADHD-C, ADHD-I, and TD is performed based on eight features such as medication status, gender, full IQ measured by Wechsler abbreviated scale of intelligence (WASI), GMV, WMV, GMV_F, and WMV_F. From Fig. 4(a-d), we observe that there are no significant variations of brain tissue volume between TD and ADHD but there is a variation among subtypes. On average,

Table 2 Parameters and hyperparameters of the proposed study

Train size	684
Test size	171
Random state	1
Cross-validation	
Stratified K-Fold	n_split: 20, random_state: 1, shuffle: True
ML classifiers	
Bagging	max_features: 8, n_estimators: 100, base_estimator: DecisionTreeClassifier() random_state: 42, base_estimator__min_samples_leaf: 1, base_estimator__min_samples_split: 2
RF	n_estimators: 100, random_state: 42, min_samples_leaf: 1, min_samples_split: 2
Extra Trees	n_estimators: 100, max_features: 8, random_state: 42, min_samples_leaf: 1, min_samples_split: 2
AdaBoost	n_estimators: 100, learning_rate: 1
GB	n_estimators: 100, random state: 42, max_depth: 3, validation_fraction: 0.1, learning_rate: 0.1 subsample: 1.0, min_samples_leaf: 1, min_samples_split: 2
XGBoost	objective: 'multi:softprob', booster: 'gbtree', colsample_bytree: 0.8, gamma: 0, learning_rate: 0.15, max_depth: 10, min_child_weight: 1, random_state: 42, subsample: 0.5, seed: 1
Voting	estimators: [('Logistic', LogisticRegression(solver = 'liblinear')), ('Tree', DecisionTreeClassifier()), ('SVM', SVC())], voting: 'hard'

we find that ADHD-I children's GMV is 1.9% higher compared to ADHD-C children, the ADHD-C children's WMV is 1.7% higher than ADHD-I children, and in the case of GMV__F of ADHD-I is 1.4% higher than ADHD-C children. The difference in average WMV_F is not signification among the subject diagnoses. Figure 4(e) shows that the full IQ of ADHD-I subjects is affected highly compared to ADHD-C subjects.

4.2 Analysis of the TD and ADHD subtypes with brain tissue volume based on medication status and gender

In statistics, the standard deviation is an important term. It is defined as a measure of the dispersion from the mean value and is given by (14),

$$\sigma = \sqrt{\frac{1}{n}\sum_{i=1}^{n}\left(x_i - \mu\right)^2} \tag{14}$$

Where σ represents the population standard deviation, n represents the number of samples in the population, x_i represents i^{th} observation in the population, and μ represents the population mean. The values of mean and standard deviation for the subject's volume of brain tissues calculated are given in Tables 3 and 4.

From Table 3, the analysis of TD and ADHD subtypes can be done based on medication status. Children of ADHD-C have a greater average GMV compared to ADHD-I and TD for both medicated and non-medicated. However, we find that TD with medication has 2.36% higher GMV than not-medicated children, and in the case of ADHD-C and ADHD-I

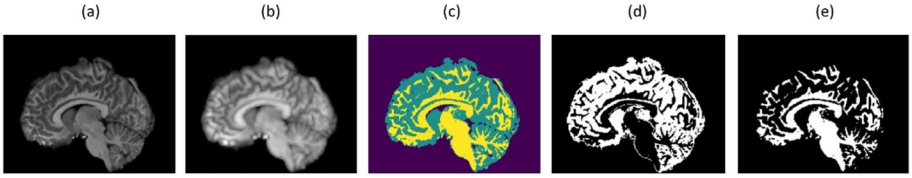

Fig. 3 (**a**) Input T1-weighted MRI (slice-91) (**b**) Filtered image (**c**) Clustered image (**d**) GM thresholded image (**e**) WM thresholded image

medicated children have approximately 2% lower GMV than not-medicated children. The WMV of ADHD-I medicated children on average was 1.7% higher compared to ADHD-C and 4.1% higher compared to TD children. There are no significant variations of GMV_F and WMV_F seen among the ADHD subtypes children.

From Table 4, children with ADHD subtypes are analyzed based on gender. The GMV on the whole in male ADHD-I children is 3.43% lower compared to children of female ADHD-I. However, in the case of ADHD-C males have 1.6% GMV lower than female children and TD male has 3% higher GMV than females. In male subjects, the GMV of ADHD-C is 3% higher than TD and 2.3% higher than ADHD-I. The WMV of ADHD-I male children is approximately 2% higher compared to ADHD-C and TD but, in female subjects, the WMV has no significant variation. There is no significant variation in GMV_F and WMV_F for both genders and among the classes or diagnoses.

4.3 Classification of TD and ADHD subtypes

A total of 85 subject records are removed due to null values and outliers. Then, we found that the ADHD-H subtype contained only 3 subjects. Hence, we limited our classification model to work on ADHD-C, ADHD-I, and TD. The dataset subjects increased to 918 subjects after augmentation. These subjects with eight features were divided with a split of 20% and 80% for testing and training datasets respectively. Accuracy (A), precision (P), recall (R), and f1-score (F) are the metrics used for evaluating the classification model [42].

$$A = \frac{TP_{TD} + TN_{TD}}{TP_{TD} + FP_{TD} + TN_{TD} + FN_{TD}} \tag{15}$$

$$P = \frac{TP_{TD}}{TP_{TD} + FP_{TD}} \tag{16}$$

$$R = \frac{TP_{TD}}{TP_{TD} + FN_{TD}} \tag{17}$$

$$F = \frac{2 \times (P \times R)}{P + R} \tag{18}$$

Where, TP_{TD} – predicted as TD for actual TD subjects, TN_{TD}– predicted as not TD for not TD subjects i.e. addition of $TP_{ADHD\text{-}C}$, $E_{ADHD\text{-}I/ADHD\text{-}C}$, $E_{ADHD\text{-}C/ADHD\text{-}I}$, and $TP_{ADHD\text{-}I}$, FP_{TD} – predicted as not TD but TD subjects i.e. $E_{ADHD\text{-}C/TD}$ and $E_{ADHD\text{-}I/TD}$, FN_{TD} – predicted as TD but not TD subjects i.e. $E_{ADHD\text{-}C/TD}$ and $E_{ADHD\text{-}I/TD}$. The dataset has three

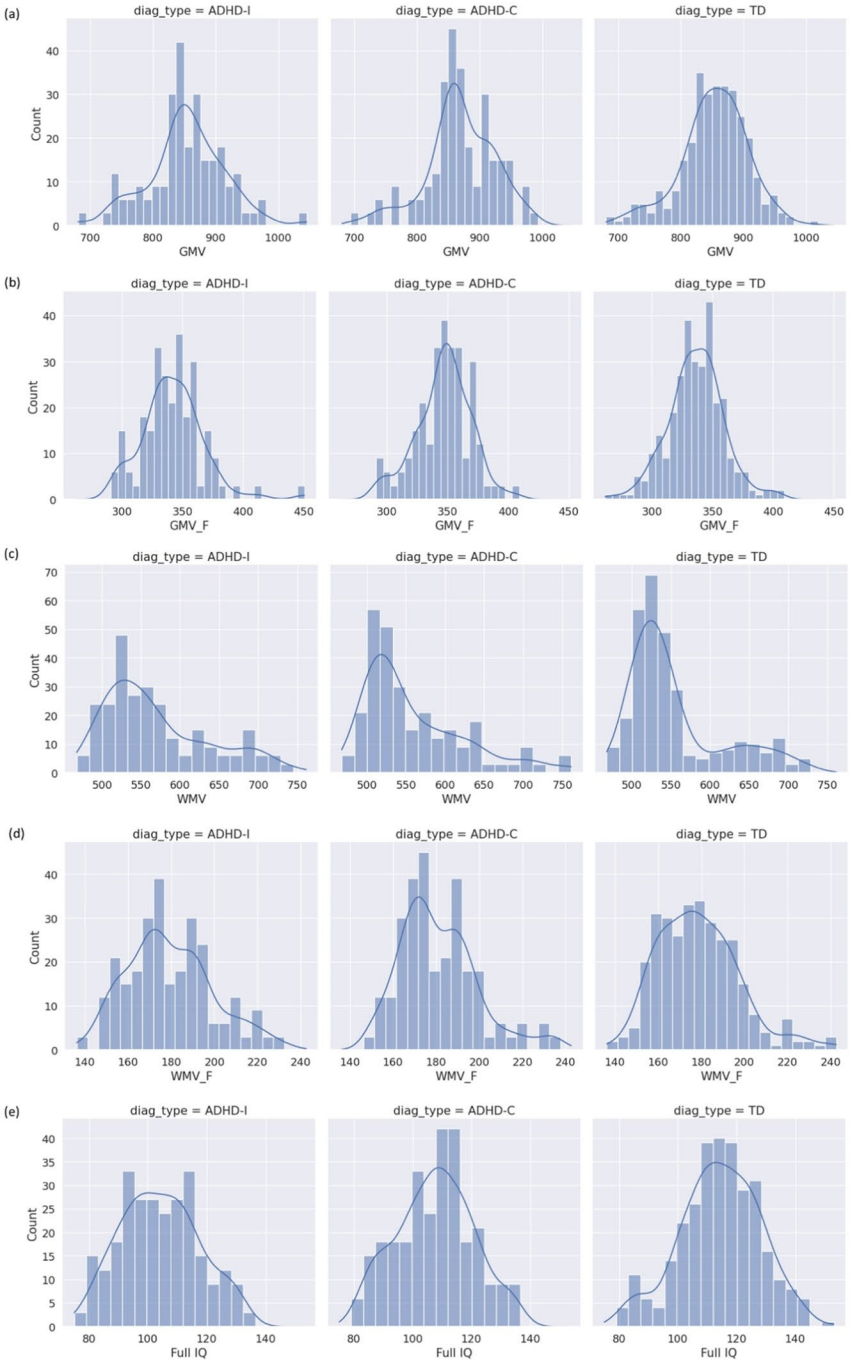

Fig. 4 Analysis of subject diagnosis with (**a**) GMV in cm^3, (**b**) WMV in cm^3, (**c**) GMV_F in cm^3, (**d**) WMV_F in cm^3, and (**e**) Full IQ

Table 3 Volume of brain tissues based on medication status

Medication Status	Diagnosis	Mean ± Standard deviation			
		GMV (in cm^3)	GMV_F (in cm^3)	WMV (in cm^3)	WMV_F (in cm^3)
Medication Naive	TD	683.8279 ± 42.50251	269.8722 ± 18.122	444.807 ± 48.15422	143.4214 ± 15.18361
	ADHD-C	690.5888 ± 49.14341	275.3378 ± 19.52421	454.9127 ± 61.05281	147.8777 ± 15.22057
	ADHD-I	678.7992 ± 47.44942	272.7138 ± 18.75405	463 ± 57.90497	144.137 ± 16.72494
Not Medication Naive	TD	667.8916 ± 34.53631	258.6467 ± 19.46016	412.3792 ± 13.76493	134.3489 ± 8.664717
	ADHD-C	704.2094 ± 34.80873	281.3852 ± 14.42765	440.6926 ± 36.60348	141.5143 ± 12.1391
	ADHD-I	695.7354 ± 50.7751	277.4969 ± 24.24384	439.2765 ± 32.3734	142.1966 ± 12.93099

Table 4 Volume of brain tissues based on gender

Gender	Diagnosis	Mean ± Standard deviation			
		GMV (in cm^3)	GMV_F (in cm^3)	WMV (in cm^3)	WMV_F (in cm^3)
Female	TD	694.5558 ± 32.77269	273.3348 ± 16.28101	433.2136 ± 38.61925	139.9941 ± 12.54609
	ADHD-C	706.0086 ± 42.92489	274.4694 ± 20.17957	430.0528 ± 35.12515	140.1458 ± 10.19224
	ADHD-I	702.4973 ± 39.92387	279.3382 ± 17.39747	430.6523 ± 48.49486	140.7048 ± 15.46214
Male	TD	673.6645 ± 47.1141	266.258 ± 19.21021	453.0657 ± 52.9375	145.8911 ± 16.5636
	ADHD-C	694.7299 ± 43.97543	278.2614 ± 17.23729	452.2528 ± 54.20819	146.0432 ± 14.77271
	ADHD-I	678.4155 ± 49.92904	272.624 ± 21.08711	463.3309 ± 52.18926	144.3756 ± 15.77525

classes, so the multiclass classification approach is used. For TD, the performance metrics can be calculated using (15), (16), (17), (18) and the confusion matrix is shown in Fig. 5. Similarly, the metrics for ADHD-I and ADHD-C subjects are calculated. Table 5 presents the values of the performance metrics acquired through the implementation of ML methods for classification. Here, the XGBoost is classifying the dataset with the highest model accuracy of 92.98%. The dataset used in the study is highly complex and has non-linear relationships between features and the target variable. Therefore, algorithms like GNB, GB, and Voting classifiers are not performing well. In Fig. 6, the confusion matrix obtained by the XGBoost classifier is shown.

Cross-validation is a crucial stage in the ML process that reduces the impact of data variability and provides a more accurate estimate of the models' performance, assisting in the development of strong, generalizable models. When choosing and evaluating models for implementation in the real world, cross-validation is an established procedure. An extension of the common cross-validation method, Stratified K-Fold (SKF) cross-validation [43] is applied in this study. The cross-validation score of each ML method is shown in Fig. 7. The highest cross-validation score of 0.9297 is attained by the XGBoost classifier.

By utilizing the SHAP for the effective classification model, the important features responsible are identified. Figure 8 shows the average impact of each feature on model output magnitude. Here, TD subjects belong to class 0, ADHD-C subjects belong to class 1, and ADHD-I subjects belong to class 2. The age and medication status of the subjects have the highest impact on the classification of ADHD-I and TD respectively. The subject's GMV, GMV_F, WMV_F, and medication status have major effects on the ADHD-C classification. Figure 9 illustrates the order of features from high to low value having an impact on the classification model. It indicates that the top four features by which ADHD subtypes and TD children are classified are medication status, full IQ, gender, and GMV.

5 Discussions

This work uses a novel method to generate brain tissue volume, and the computed volumes were combined with the subject's phenotypic information. In previous research, toolboxes were used to analyze brain volume to distinguish between TD and ADHD. However, not all operating systems are supported by these toolboxes. Therefore, the volume of brain tissues is calculated in the proposed study using an algorithm. The average GM and WM volumes of the subjects calculated are 856.0368cm^3 and 557.9337cm^3 respectively. We find

Fig. 5 Confusion matrix for TD, ADHD-C, and ADHD-I

PREDICTED CLASS	TRUE CLASS: TD	TRUE CLASS: ADHD-C	TRUE CLASS: ADHD-I
TD	TP_{TD}	$E_{ADHD\text{-}C/TD}$	$E_{ADHD\text{-}I/TD}$
ADHD-C	$E_{TD/ADHD\text{-}C}$	$TP_{ADHD\text{-}C}$	$E_{ADHD\text{-}I/ADHD\text{-}C}$
ADHD-I	$E_{TD/ADHD\text{-}I}$	$E_{ADHD\text{-}C/ADHD\text{-}I}$	$TP_{ADHD\text{-}I}$

Table 5 Comparison of ML methods for ADHD subtypes and TD classification

Method	Performance metrics	Diagnosis			Model Accuracy
		TD	ADHD-I	ADHD-C	
Random forest	precision	0.9333	0.8573	0.9354	90.64%
	recall	0.7636	1.0000	0.9508	
	f1-score	0.8400	0.9243	0.9430	
Bagging	precision	0.9333	0.8461	0.9508	90.64%
	recall	0.7636	1.0000	0.9508	
	f1-score	0.8400	0.9166	0.9508	
XGBoost	**precision**	**0.9387**	**0.9166**	**0.9355**	**92.98%**
	recall	**0.8363**	**1.0000**	**0.9508**	
	f1-score	**0.8846**	**0.9565**	**0.9431**	
Adaboost	precision	0.6406	0.6071	0.7058	64.91%
	recall	0.7454	0.6181	0.5901	
	f1-score	0.6890	0.6126	0.6428	
GB	precision	0.8400	0.8474	0.8871	85.96%
	recall	0.7636	0.9090	0.9016	
	f1-score	0.8000	0.8772	0.8943	
Voting	precision	0.4444	0.7894	0.9200	59.06%
	recall	0.8727	0.5454	0.3770	
	f1-score	0.5889	0.6451	0.5349	
GNB	precision	0.5404	0.6059	0.4576	50.88%
	recall	0.8526	0.4537	0.2621	
	f1-score	0.6615	0.5189	0.3333	
Extra Trees	precision	0.9361	0.9016	0.9206	91.81%
	recall	0.8000	1.0000	0.9508	
	f1-score	0.8627	0.9482	0.9354	

that these values are similar to the values given in BIC Template Brain [44]. In most of the existing research [45–49], voxel-based morphometry (VBM) is used which is a common technique to analyze volumetric differences across the entire brain. Nevertheless, it is questioned because of potential confounds. In [50], the author has done an analysis of VBM and manual regions of interest. Here, they identified that VBM was correctly identifying only a few brain regions. Also, suggested that both methods measure the same effects

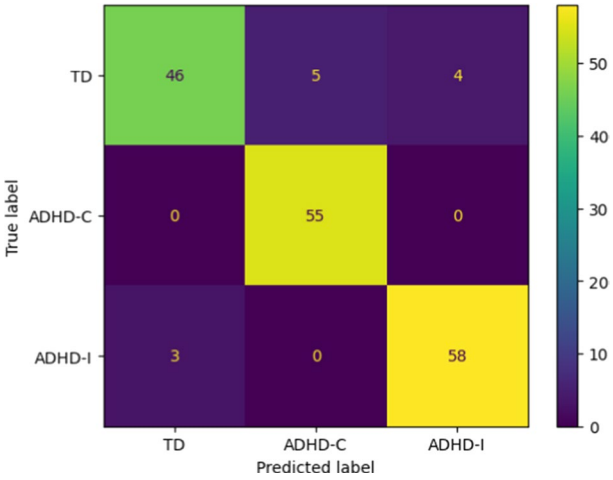

Fig. 6 Confusion matrix obtained by the XGBoost Classifier

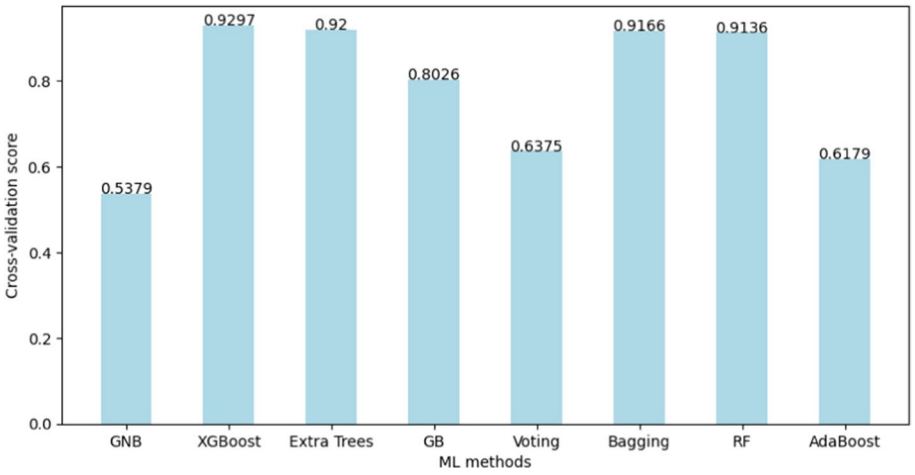

Fig. 7 Cross-validation score obtained by different ML methods applying SKF cross-validation

concerning subcortical brain structures. This motivated us to make use of FCM-based segmentation and calculate the volume of segmented brain tissues.

A few similar existing work contributions are discussed in the following: In [51], the brain volume was analyzed based on gender. They contributed that ADHD boys have reduced volume compared to TD boys while ADHD girls show higher volume compared to TD girls in the ventral anterior cingulate cortex. Here, the number of subjects used for the study was 60 among which there were 27 TD and 33 ADHD-C children who weren't taking medication. In [52], the authors compared children with ADHD, ASD, and TD based on the development coordination disorder questionnaire (DCDQ). Fifty-five children in the age groups of 8 to 12 were included in this study. DCDQ scores are calculated using coordination, fine motor skills, handwriting, and movement control. The association between the DCDQ score and six regional volume abnormalities is explored within each group of children. They observed that in the group of people with ASD, the volume of the right medial frontal gyrus was related to

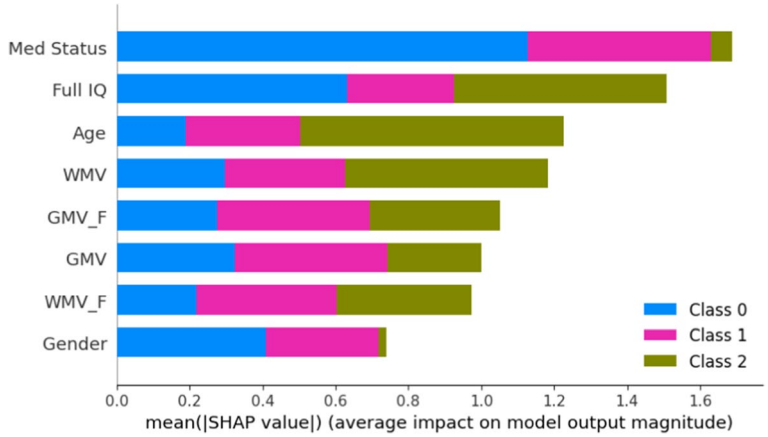

Fig. 8 SHAP showing the average impact of each feature on model output magnitude

coordination skills. In children with ADHD, the volume of the right superior frontal gyrus was correlated with the overall DCDQ score. In [53], the authors investigated T1 and T2 weighted MRI of 27 healthy controls and 37 drug-free ADHD children. This study used a Pearson correlation analysis. The results show that the GM regions in children with ADHD have different brain structures from TD in the cerebellum, the attention and execution control network, and the limbic system. This study analyzed TD and ADHD subtypes of children's brain volume based on medication status and gender.

The various ML methods were investigated and the efficient model was identified as XGBoost. The inference obtained after applying SHAP is that brain GMV, WMV, and GMV_F are significant in the classification of ADHD subtypes along with medication status and full IQ. Table 6 presents a comparison of the proposed approach with the existing research results. The proposed approach with the XGBoost classifier can classify between ADHD and TD with an accuracy of 90.64%. This indicates a 6.64% and 15.64% increase in accuracy when compared to the research performed in references [27, 28] respectively, using sMRI.

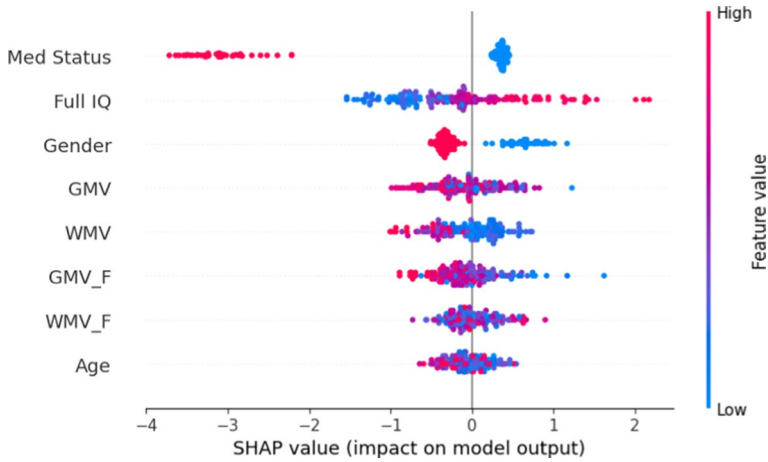

Fig. 9 SHAP showing the impact of features in the classification of ADHD subtypes

Table 6 Comparison of existing research with the proposed work in the classification of ADHD

Author/Year	Method	Result	Dataset	Imaging modality
Peng X et al. / 2013 [54]	Extreme learning machine and SVM	Classification accuracy for ELM is 90.18% and SVM-84.73%	ADHD200 (ADHD-55 and Control-56)	Structural MRI
Tenev A et al./2014 [55]	SVM	Classification accuracy for ADHD subtypes is 90% and ADHD versus control is 70%	ADHD-67 and Control-50	EEG recording
Junqiang Du et al. / 2016 [56]	SVM	Accuracy-94.91% Sensitivity-93.22% Specificity-96.94%	ADHD200 (ADHD-118 and Control-98)	Functional MRI
Atif Riaz et al. / 2018 [57]	SVM	Maximum accuracy of 86.7% attained by KKI imaging site	ADHD200	Functional MRI
Kautzky A. et al. / 2020 [21]	Random forest	Accuracy- 82% Sensitivity-75% Specificity-86%	ADHD-16 and controls-22 collected from the Medical University of Vienna	PET
Mikolas P. et al. / 2022 [58]	SVM	Accuracy-66% Sensitivity-66.9% Specificity-65.4%	299 participants at the Medical faculty of the Technical Dresden, Germany	Medical records
Maniruzzaman M et al. / 2022 [59]	LASSO with SVM	Accuracy-94.2% Sensitivity-93.3% F1 score-91.99%	ADHD-28 Controls-24	EEG
SainiS. et al. / 2022 [60]	k-nearest neighbors (kNN)	Classification accuracy-89%	ADHD-77 and Controls-80 from IEEE Dataport	EEG
ShinJ. et al. / 2023 [61]	Random forest	Classification accuracy-93.1%	29 samples from Japanese school	Handwriting patterns using a pen tablet
Chauhan et al. / 2023 [27]	Naïve Bayes	Classification accuracy-84%	ADHD-60 and Controls-60	EEG
Dhruv Chandra Lohani et al. / 2023[28]	Radial-based SVM and linear SVM	Classification accuracy-75%	ADHD200 (ADHD-316 and Controls-316)	Structural MRI and personal characteristics
Proposed work	XGBoost classifier	Classification accuracy for ADHD subtypes and TD is 92.98% ADHD versus TD is 90.64%	ADH200 (TD-306, ADHD-C-94, and ADHD-I-89)	Structural MRI and phenotypic information

6 Conclusion

The highest model accuracy of 92.98% is obtained by the proposed approach using the XGBoost classifier for ADHD subtypes and TD. This classification model can help identify subtypes of ADHD based on various features such as medication status, gender, full IQ score, age, GMV_F, GMV, WMV_F, and WMV. The most common tools such as Freesurfer and FMRIB Software Library (FSL) used in brain tissue segmentation do not support the Windows operating system [62]. Therefore, this study introduced a method that segments the brain tissue and calculates the volume of the important brain tissues without the use of neuroimaging tools available online. This approach had the benefit of being compatible with all operating systems. Furthermore, the most important features in the classification of ADHD subtypes and TD were identified by the SHAP. This can help prioritize further research and inform the clinical assessment. It is important to acknowledge the limitations of the study, including potential biases in the data and the need to validate the findings in diverse populations.

Future studies can focus on enhancing and optimizing the ML algorithms utilized for classifying ADHD subtypes. A possible approach is to investigate various feature selection techniques, model structures, and hyperparameter optimization methods to enhance classification precision and applicability to various populations. Also, Longitudinal data can be used with these machine learning methods to predict treatment response, symptom progression, and functional results. This lets doctors act quickly and make personalized treatment plans. Classification systems could also work more effectively if they used data from a variety of sources, such as neuroimaging, genetic markers, cognitive tests, and behavioral observations. Integrating diverse data sources can provide a more comprehensive understanding of the underlying neurobiological mechanisms associated with ADHD subtypes.

Acknowledgments The ADHD-200 online dataset was made available by the NeuroImaging Tools and Resources Collaboratory (http://www.NITRC.org), for which the authors are thankful. We would like to thank the SRM Medical College Hospital and Research Centre for granting us the Ethical Clearance Number: 8464/IEC2022 to collect childrens' brain MRI scans.

Funding The authors of the research declare that no grants, funding, or other forms of support were offered.

Data availability Visit https://fcon_1000.projects.nitrc.org/indi/adhd200/ to get the ADHD-200 dataset.

Declarations

Ethics approval and consent to participate Not Applicable.

Conflict of interest There are no disclosed possible conflicts of interest for the contributors.

References

1. Salari N, Ghasemi H, Abdoli N, Rahmani A, Shiri MH, Hashemian AH, Akbari H, Mohammadi M (2023) The global prevalence of ADHD in children and adolescents: a systematic review and meta-analysis. Ital J Pediatr 49(1):48. https://doi.org/10.1186/s13052-023-01456-1
2. Roehr B (2013) American psychiatric association explains DSM-5. Bmj 346. https://doi.org/10.1136/bmj.f3591
3. Kostick K (2017) ICD-10-CM coding for attention-deficit/hyperactivity disorder (ADHD). J AHIMA 88(9):56–59

4. Cabral MD, Liu S, Soares N (2020) Attention-deficit/hyperactivity disorder: diagnostic criteria, epidemiology, risk factors and evaluation in youth. Transl Pediatr 9(Suppl 1):S104. https://doi.org/10.21037/tp.2019.09.08
5. Honkasilta J, Koutsoklenis A (2022) The (un) real existence of ADHD—criteria, functions, and forms of the diagnostic entity. Front Sociol 7:814763. https://doi.org/10.3389/fsoc.2022.814763
6. Champ RE, Adamou M, Tolchard B (2021) The impact of psychological theory on the treatment of attention deficit hyperactivity disorder (ADHD) in adults: a scoping review. PLoS One 16(12):e0261247. https://doi.org/10.1371/journal.pone.0261247
7. Zysset A, Robin D, Albermann K, Dratva J, Hotz S, Wieber F, von Rhein M (2023) Diagnosis and management of ADHD: a pediatric perspective on practice and challenges in Switzerland. BMC Pediatr 23(1):1–2. https://doi.org/10.1186/s12887-023-03873-x
8. Anita S, Aruna Priya P (2020) Diagnosis of Parkinson's disease at an early stage using volume rendering SPECT image slices. Arab J Sci Eng 45(4):2799–2811. https://doi.org/10.1007/s13369-019-04152-7
9. Yen C, Lin CL, Chiang MC (2023) Exploring the frontiers of neuroimaging: a review of recent advances in understanding brain functioning and disorders. Life 13(7):1472. https://doi.org/10.3390/life13071472
10. Shoeibi A, Khodatars M, Jafari M, Ghassemi N, Moridian P, Alizadesani R, Ling SH, Khosravi A, Alinejad-Rokny H, Lam HK, Fuller-Tyszkiewicz M (2022) Diagnosis of brain diseases in fusion of neuroimaging modalities using deep learning: a review. Inf Fusion. https://doi.org/10.1016/j.inffus.2022.12.010
11. Pateria N, Kumar D (2023) A comprehensive review on detection and classification of dementia using neuroimaging and machine learning. Multimed Tools Appl:1–39. https://doi.org/10.1007/s11042-023-17288-4
12. Halder A, Talukdar NA (2023) Kernel induced semi-supervised spatial clustering: a novel brain MRI segmentation technique. Multimed Tools Appl:1–29. https://doi.org/10.1007/s11042-023-16806-8
13. Pilli R, Goel T, Murugan R, Tanveer M (2023)https://www.ncbi.nlm.nih.gov/books/NBK553239/
14. Mercadante AA, Tadi P (2020) Neuroanatomy, gray matter. StatPearls Publishing. Available from:https://www.ncbi.nlm.nih.gov/books/NBK553239/
15. Teleanu RI, Niculescu AG, Roza E, Vladâcenco O, Grumezescu AM, Teleanu DM (2022) Neurotransmitters—key factors in neurological and neurodegenerative disorders of the central nervous system. Int J Mol Sci 23(11):5954. https://doi.org/10.3390/ijms23115954
16. Patel PK, Leathem LD, Currin DL, Karlsgodt KH (2021) Adolescent neurodevelopment and vulnerability to psychosis. Biol Psychiatry 89(2):184–193. https://doi.org/10.1016/j.biopsych.2020.06.028
17. Long Y, Pan N, Ji S, Qin K, Chen Y, Zhang X, He M, Suo X, Yu Y, Wang S, Gong Q (2022) Distinct brain structural abnormalities in attention-deficit/hyperactivity disorder and substance use disorders: a comparative meta-analysis. Transl Psychiatry 12(1):368. https://doi.org/10.1038/s41398-022-02130-6
18. Lee MM, Drury BC, McGrath LM, Stoodley CJ (2023) Shared grey matter correlates of reading and attention. Brain Lang 237:105230. https://doi.org/10.1016/j.bandl.2023.105230
19. Damatac CG, Chauvin RJ, Zwiers MP, van Rooij D, Akkermans SE, Naaijen J, Hoekstra PJ, Hartman CA, Oosterlaan J, Franke B, Buitelaar JK (2022) White matter microstructure in attention-deficit/hyperactivity disorder: a systematic tractography study in 654 individuals. Biol Psychiatry Cogn Neurosci Neuroimaging 7(10):979–988. https://doi.org/10.1016/j.bpsc.2020.07.015
20. Zhao Y, Yang L, Gong G, Cao Q, Liu J (2022) Identify aberrant white matter microstructure in ASD, ADHD and other neurodevelopmental disorders: a meta-analysis of diffusion tensor imaging studies. Prog Neuro-Psychopharmacol Biol Psychiatry 113:110477. https://doi.org/10.1016/j.pnpbp.2021.110477
21. Kautzky A, Vanicek T, Philippe C, Kranz GS, Wadsak W, Mitterhauser M, Hartmann A, Hahn A, Hacker M, Rujescu D, Kasper S (2020) Machine learning classification of ADHD and HC by multimodal serotonergic data. Transl Psychiatry 10(1):104. https://doi.org/10.1038/s41398-020-0781-2
22. Parashar A, Kalra N, Singh J, Goyal RK (2021) Machine learning based framework for classification of children with adhd and healthy controls. Intell Autom Soft Comput 28(3):669–682. https://doi.org/10.32604/iasc.2021.017478
23. Slobodin O, Yahav I, Berger I (2020) A machine-based prediction model of ADHD using CPT data. Front Hum Neurosci 14:560021. https://doi.org/10.3389/fnhum.2020.560021
24. Shao L, Zhang D, Du H, Fu D (2019) Deep forest in ADHD data classification. IEEE Access 7:137913–137919. https://doi.org/10.1109/ACCESS.2019.2941515

25. Shao L, You Y, Du H, Fu D (2020) Classification of ADHD with fMRI data and multi-objective optimization. Comput Methods Prog Biomed 196:105676. https://doi.org/10.1016/j.cmpb.2020.105676
26. Chen Y, Tang Y, Wang C, Liu X, Zhao L, Wang Z (2020) ADHD classification by dual subspace learning using resting-state functional connectivity. Artif Intell Med 103:101786. https://doi.org/10.1016/j.artmed.2019.101786
27. Chauhan N, Choi BJ (2023) Regional contribution in electrophysiological-based classifications of attention deficit hyperactive disorder (ADHD) using machine learning. Computation 11(9):180. https://doi.org/10.3390/computation11090180
28. Lohani DC, Rana B (2023) ADHD diagnosis using structural brain MRI and personal characteristic data with machine learning framework. Psychiatry Res Neuroimaging 334:111689. https://doi.org/10.1016/j.pscychresns.2023.111689
29. Gao Y, Ni H, Chen Y, Tang Y, Liu X (2023) Subtype classification of attention deficit hyperactivity disorder with hierarchical binary hypothesis testing framework. J Neural Eng 20(5):056015. https://doi.org/10.1088/1741-2552/acf523
30. Lin IC, Chang SC, Huang YJ, Kuo TB, Chiu HW (2023) Distinguishing different types of attention deficit hyperactivity disorder in children using artificial neural network with clinical intelligent test. Front Psychol 13:1067771. https://doi.org/10.3389/fpsyg.2022.1067771
31. Ahmadi A, Kashefi M, Shahrokhi H, Nazari MA (2021) Computer aided diagnosis system using deep convolutional neural networks for ADHD subtypes. Biomed Signal Process Control 63:102227. https://doi.org/10.1016/j.bspc.2020.102227
32. Bellec P, Chu C, Chouinard-Decorte F, Benhajali Y, Margulies DS, Craddock RC (2017) The neuro bureau ADHD-200 preprocessed repository. Neuroimage 144:275–286. https://doi.org/10.1016/j.neuroimage.2016.06.034
33. Smith SM (2002) Fast robust automated brain extraction. Hum Brain Mapp 17(3):143–155. https://doi.org/10.1002/hbm.10062
34. Zhang Y, Brady M, Smith S (2001) Segmentation of brain MR images through a hidden Markov random field model and the expectation-maximization algorithm. IEEE Trans Med Imaging 20(1):45–57. https://doi.org/10.1109/42.906424
35. Jenkinson M, Bannister P, Brady M, Smith S (2002) Improved optimization for the robust and accurate linear registration and motion correction of brain images. Neuroimage 17(2):825–841. https://doi.org/10.1006/nimg.2002.1132
36. Andersson JL, Jenkinson M, Smith S (2007) Non-linear registration, aka spatial normalisation FMRIB technical report TR07JA2. FMRIB Analysis Group of the University of Oxford 2(1):e21.
37. Chen Z, Zwiggelaar R (2010) A modified fuzzy c-means algorithm for breast tissue density segmentation in mammograms. In Proceedings of the 10th IEEE International Conference on Information Technology and Applications in Biomedicine 1–4. https://doi.org/10.1109/ITAB.2010.5687751
38. Marutho D, Handaka SH, Wijaya E (2018) The determination of cluster number at k-mean using elbow method and purity evaluation on headline news. In 2018 international seminar on application for technology of information and communication 533-538. https://doi.org/10.1109/ISEMANTIC.2018.8549751
39. Szilagyi L, Benyo Z, Szilágyi SM, Adam HS (2003) MR brain image segmentation using an enhanced fuzzy c-means algorithm. In Proceedings of the 25th annual international conference of the IEEE engineering in medicine and biology society (IEEE Cat. No. 03CH37439) 724-726. https://doi.org/10.1109/IEMBS.2003.1279866
40. Feng W, Gou J, Fan Z, Chen X (2023) An ensemble machine learning approach for classification tasks using feature generation. Connect Sci 35(1):2231168. https://doi.org/10.1080/09540091.2023.2231168
41. Molnar C (2020) Interpretable machine learning - a guide for making black box models explainable. https://christophm.github.io/interpretable-ml-book/
42. Quasar SR, Sharma R, Mittal A, Sharma M, Agarwal D, de La Torre DI (2023) Ensemble methods for computed tomography scan images to improve lung cancer detection and classification. Multimed Tools Appl:1–31. https://doi.org/10.1007/s11042-023-17616-8
43. Prusty S, Patnaik S, Dash SK (2022) SKCV: stratified K-fold cross-validation on ML classifiers for predicting cervical cancer. Front Nanotechnol 4:972421. https://doi.org/10.3389/fnano.2022.972421
44. Noor Kabani (1998) Brain volume. http://www.bic.mni.mcgill.ca/users/noor/brain_volume.html
45. Vilgis V, Sun L, Chen J, Silk TJ, Vance A (2016) Global and local grey matter reductions in boys with ADHD combined type and ADHD inattentive type. Psychiatry Res Neuroimaging 254:119–126. https://doi.org/10.1016/j.pscychresns.2016.06.008
46. Lim L, Chantiluke K, Cubillo AI, Smith AB, Simmons A, Mehta MA, Rubia K (2015) Disorder-specific grey matter deficits in attention deficit hyperactivity disorder relative to autism spectrum disorder. Psychol Med 45(5):965–976. https://doi.org/10.1017/S0033291714001974

47. Villemonteix T, De Brito SA, Kavec M, Balériaux D, Metens T, Slama H, Baijot S, Mary A, Peigneux P, Massat I (2015) Grey matter volumes in treatment naïve vs. chronically treated children with attention deficit/hyperactivity disorder: a combined approach. Eur Neuropsychopharmacol 25(8):1118–1127. https://doi.org/10.1016/j.euroneuro.2015.04.015
48. Fu C, Chen S, Qian A, Zhou R, Zhou J, Li J, Cheng J, Yang C, Zhao K, Wang M (2021) Larger thalamus correlated with inattentive severity in the inattentive subtype of ADHD without comorbidity. Psychiatry Res 304:114079. https://doi.org/10.1016/j.psychres.2021.114079
49. Fernandez L, Burmester A, Duque JD, Silk TJ, Hyde CE, Kirkovski M, Enticott PG, Caeyenberghs K (2023) Examination of cerebellar grey-matter volume in children with neurodevelopmental disorders: a coordinated analysis using the ACAPULCO algorithm. Cerebellum 22(6):1243–1249. https://doi.org/10.1007/s12311-022-01503-3
50. Focke NK, Trost S, Paulus W, Falkai P, Gruber O (2014) Do manual and voxel-based morphometry measure the same? A proof of concept study. Front Psychiatry 5:39. https://doi.org/10.3389/fpsyt.2014.00039
51. Villemonteix T, De Brito SA, Slama H, Kavec M, Balériaux D, Metens T, Baijot S, Mary A, Peigneux P, Massat I (2015) Grey matter volume differences associated with gender in children with attention-deficit/hyperactivity disorder: a voxel-based morphometry study. Dev Cogn Neurosci 14:32–37. https://doi.org/10.1016/j.dcn.2015.06.001
52. Albajara Sáenz A, Villemonteix T, Van Schuerbeek P, Baijot S, Septier M, Defresne P, Delvenne V, Passeri G, Raeymaekers H, Victoor L, Willaye E (2021) Motor abnormalities in attention-deficit/hyperactivity disorder and autism spectrum disorder are associated with regional grey matter volumes. Front Neurol 12:666980. https://doi.org/10.3389/fneur.2021.666980
53. Su S, Chen Y, Dai Y, Lin L, Qian L, Zhou Q, Zou M, Zhang H, Liu M, Xiang X, Yang Z (2021) Quantitative synthetic MRI reveals grey matter abnormalities in children with drug-naïve attention-deficit/hyperactivity disorder. Brain Imaging Behav:1–9. https://doi.org/10.1007/s11682-021-00514-8
54. Peng X, Lin P, Zhang T, Wang J (2013) Extreme learning machine-based classification of ADHD using brain structural MRI data. PLoS One 8(11):e79476. https://doi.org/10.1371/journal.pone.0079476
55. Tenev A, Markovska-Simoska S, Kocarev L, Pop-Jordanov J, Müller A, Candrian G (2014) Machine learning approach for classification of ADHD adults. Int J Psychophysiol 93(1):162–166. https://doi.org/10.1016/j.ijpsycho.2013.01.008
56. Du J, Wang L, Jie B, Zhang D (2016) Network-based classification of ADHD patients using discriminative subnetwork selection and graph kernel PCA. Comput Med Imaging Graph 52:82–88. https://doi.org/10.1016/j.compmedimag.2016.04.004
57. Riaz A, Asad M, Alonso E, Slabaugh G (2018) Fusion of fMRI and non-imaging data for ADHD classification. Comput Med Imaging Graph 65:115–128. https://doi.org/10.1016/j.compmedimag.2017.10.002
58. Mikolas P, Vahid A, Bernardoni F, Süß M, Martini J, Beste C, Bluschke A (2022) Training a machine learning classifier to identify ADHD based on real-world clinical data from medical records. Sci Rep 12(1):12934. https://doi.org/10.1038/s41598-022-17126-x
59. Maniruzzaman M, Shin J, Hasan MA, Yasumura A (2022) Efficient feature selection and machine learning based ADHD detection using EEG signal. Comput Mater Contin 72(3). https://doi.org/10.32604/cmc.2022.028339
60. Saini S, Rani R, Kalra N (2022) Prediction of attention deficit hyperactivity disorder (ADHD) using machine learning techniques based on classification of EEG signal. In 2022 8th International Conference on Advanced Computing and Communication Systems (ICACCS) 782-786. https://doi.org/10.1109/ICACCS54159.2022.9785356.
61. Shin J, Maniruzzaman M, Uchida Y, Hasan MA, Megumi A, Yasumura A (2023) Handwriting-based ADHD detection for children having ASD using machine learning approaches. IEEE Access. https://doi.org/10.1109/ACCESS.2023.3302903
62. Singh MK, Singh KK (2021) A review of publicly available automatic brain segmentation methodologies, machine learning models, recent advancements, and their comparison. Ann Neurosci 28(1–2):82–93. https://doi.org/10.1177/09727531211990175